AGU PUBLICATIONS

Geophysical Research Letters

RESEARCH LETTER
10.1002/2014GL062347

Key Points:
- Tide modulations of the microseismic energy are observed at shoreline stations
- Coastal and open-sea microseismic sources coexist in different frequency ranges
- Most of the 2–5 s period microseisms on the Atlantic coast come from deep ocean

Supporting Information:
- Text S1
- Figure S1
- Figure S2
- Figure S3
- Figure S4
- Figure S5
- Figure S6
- Figure S7

Correspondence to:
É. Beucler,
eric.beucler@univ-nantes.fr

Citation:
Beucler, É., A. Mocquet, M. Schimmel, S. Chevrot, O. Quillard, J. Vergne, and M. Sylvander (2015), Observation of deep water microseisms in the North Atlantic Ocean using tide modulations, *Geophys. Res. Lett.*, *42*, 316–322, doi:10.1002/2014GL062347.

Received 27 OCT 2014
Accepted 19 DEC 2014
Accepted article online 28 DEC 2014
Published online 23 JAN 2015

Observation of deep water microseisms in the North Atlantic Ocean using tide modulations

Éric Beucler[1], Antoine Mocquet[1], Martin Schimmel[2], Sébastien Chevrot[3], Olivier Quillard[1], Jérôme Vergne[4], and Matthieu Sylvander[3]

[1]Laboratoire de Planétologie et Géodynamique, CNRS UMR 6112, Université de Nantes, France, [2]Department of Structure and Dynamics of the Earth, Institute of Earth Sciences Jaume Almera, Consejo Superior de Investigaciones Científicas, Barcelona, Spain, [3]Institut de Recherche en Astrophysique et Planétologie, CNRS UMR 5277, Toulouse, France, [4]EOST, CNRS UMR 7516, Strasbourg, France

Abstract Ocean activity produces continuous and ubiquitous seismic energy mostly in the 2–20 s period band, known as microseismic noise. Between 2 and 10 s period, secondary microseisms (SM) are generated by swell reflections close to the shores and/or by opposing swells in the deep ocean. However, unique conditions are required in order for surface waves generated by deep-ocean microseisms to be observed on land. By comparing short-duration power spectral densities at both Atlantic shoreline and inland seismic stations, we show that ocean tides strongly modulate the seismic energy in a wide period band except between 2.5 and 5 s. This tidal proxy reveals the existence of an ex situ short-period contribution of the SM peak. Comparison with swell spectra at surrounding buoys suggests that the largest part of this extra energy comes from deep ocean-generated microseisms. The energy modulation might be also used in numerical models of microseismic generation to constrain coastal reflection coefficients.

1. Introduction

First observations of the seismic energy gain between 2 and 20 s period, defining the microseismic noise frequency band, go back to the nineteenth century [*Bertelli*, 1872; *Wiechert*, 1904]. See *Ebeling* [2012] for a review of historical research on microseisms. This ubiquitous microseismic noise peaks at two frequencies, defining two distinct processes linking oceanic swells and microseisms [*Bernard*, 1990; *Peterson*, 1993; *Aster et al.*, 2008]. Although Earth's seismic hum can be considered as a third peak [*Webb*, 2007], it is usually attributed to long-period infragravity (IG) waves [*Kobayashi and Nishida*, 1998; *Rhie and Romanowicz*, 2004], which is different from the microseisms discussed in this paper. Primary microseisms (PM) lay within the 12–17 s period band, both on land and on the ocean bottom [*Bromirski et al.*, 2005]. Their frequencies are controlled by the dominant frequency of ocean waves that reach the shallow coastal waters [*Haubrich and McCamy*, 1969; *Gerstoft and Tanimoto*, 2007]. Secondary microseisms (SM) are characterized by a more energetic and broader peak in the 2–10 s period band, thus at approximately twice the frequency of ocean waves [*Oliver and Page*, 1963]. SM can be generated in both shallow and deep waters [*Cessaro*, 1994; *Webb*, 1998; *Chevrot et al.*, 2007] by a mechanism of nonlinear interactions of oceanic waves propagating in opposite directions generating water pressure oscillations (gravity waves) which convert efficiently into seismic waves while hitting the ocean floor [*Longuet-Higgins*, 1950; *Hasselmann*, 1963]. The most frequent location for such opposing swells is near costal surf zone close to the receiver [*Bromirski and Duennebier*, 2002; *Tanimoto*, 2007]. Many observations also report temporary open-sea SM sources during storms [*Oliver and Page*, 1963; *Cessaro*, 1994; *Chevrot et al.*, 2007; *Gerstoft and Tanimoto*, 2007; *Obrebski et al.*, 2012]. Seasonal variations of microseismic noise are observed worldwide [*Rhie and Romanowicz*, 2004; *Stutzmann et al.*, 2009; *Schimmel et al.*, 2011], with the most energetic sources alternatively located in the Northern and Southern Hemispheres, during their respective winter seasons. Some ocean bottom seismometer studies in the Pacific Ocean [*Stephen et al.*, 2003; *Bromirski et al.*, 2005] propose to divide the SM (also called DF for double-frequency) peak into long period for the sources resulting from wave interactions in shallow water and short period for the microseisms generated in the deep ocean (i.e., in the vicinity of the bottom sensor). However, a variability of oceanic swells is observed with a strong influence of bathymetry on the excitation of microseisms by resonance in the water column [*Kedar et al.*, 2008] which makes this distinction

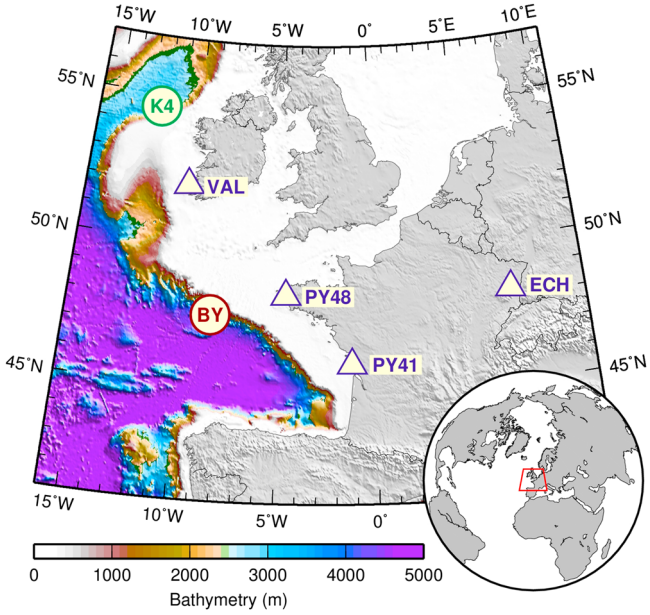

Figure 1. Location of seismic stations and buoys. PY41 and PY48 are temporary stations deployed less than 150 m from the French Atlantic tideline, both on hard rock. VAL station (Irish National Seismic Network) is located about 3 km from the Irish coast and ECH (Geoscope) is taken as a reference inland seismometer. BY (Brittany) and K4 buoys are maintained by the UK Met Office.

not applicable worldwide. Recent seismic noise modeling [*Ardhuin et al.*, 2011; *Stutzmann et al.*, 2012; *Ardhuin and Herbers*, 2013; *Sergeant et al.*, 2013] indicates that coastal reflections can be neglected for periods shorter than 7 s. Both coastal and deep water sources can therefore coexist, but some studies conclude that SM recorded on land are dominated by near-coastal wave activity [*Bromirski et al.*, 2013; *Ying et al.*, 2014]. However, seasonal variability leads to a variety of microseismic energy distributions over the frequency range, whatever the distance to the shorelines [*Kedar*, 2011]. Therefore, finding a proxy to investigate the relationships between frequency and location of microseism sources may lead to a better discrimination of the different types of SM. Here we exploit the strong tide modulations of the seismic energy, previously detected at other places [e.g., *Okihiro and Guza*, 1995; *Thomson et al.*, 2006], and we compare observations of continuous microseismic signals recorded at both coastal and inland stations.

Two of the four broadband seismic stations (PY41 and PY48) considered in this study were deployed during the 3 year PYRenean Observational Portable Experiment (PYROPE) experiment [*Chevrot et al.*, 2014]. They were both installed on hard rock, less than 150 m inland from the tideline (Figure 1). PY41 was located inside a seventeenth century citadel surrounded by a quiet tidal bay, while PY48 was installed inside a blockhaus of the second world war, built on a sandstone cliff. The tide along this coast is mostly semidiurnal [*Llubes et al.*, 2008; *Fund et al.*, 2012] with large tidal ranges of approximately 0.5–6.5 m. VAL is a permanent broadband station in the Irish network, Southwest coast of Ireland, 3 km inland. The tidal range at the nearest shore is smaller (1–3.5 m). The Geoscope station ECH [*Romanowicz et al.*, 1984], about 750 km away from the Atlantic Ocean, is taken as a reference as a typical inland station. Two UK Met Office buoys located in the northern Atlantic are also used (Figure 1). Brittany (hereafter referred to as BY) and K4 buoys are located in the deep ocean above approximately 2260 m and 2950 m of water height, respectively. Their distance from the nearest shores are of 180 km for K4 and 310 km for BY.

2. Short-Duration Power Spectral Densities

For each seismic station component short-duration power spectral densities (PSDs) are computed in the 0.2–70 s period band. We preprocess the time series by cutting the continuous signal into 360 s length time windows, with an overlap of 60 s. After removing the instrument response each record is transformed to acceleration between 10 mHz and 10 Hz. A Fourier transform algorithm is used to convert energy into $10\log_{10}((\mathrm{m/s^2})^2/\mathrm{Hz})$, which is equivalent to decibel. The final PSD values are computed by taking the median of four successive power spectra, which gives a measure of seismic power every 20 min. Comparisons with standard PSD packages assess the data processing quality [*McNamara and Boaz*, 2006]. Since earthquakes are not removed, they produce spikes visible for the whole frequency band at all stations. The spectrograms of the vertical components are displayed in Figure 2, for a time window running from 12 to 29 April 2012. Locally predicted tidal ranges, computed by the French Naval Hydrographic and Oceanographic Service, are superimposed on the PY41 and PY48 spectrograms. The corresponding spectrograms for the horizontal components are displayed in Figures S1 and S2 in the supporting

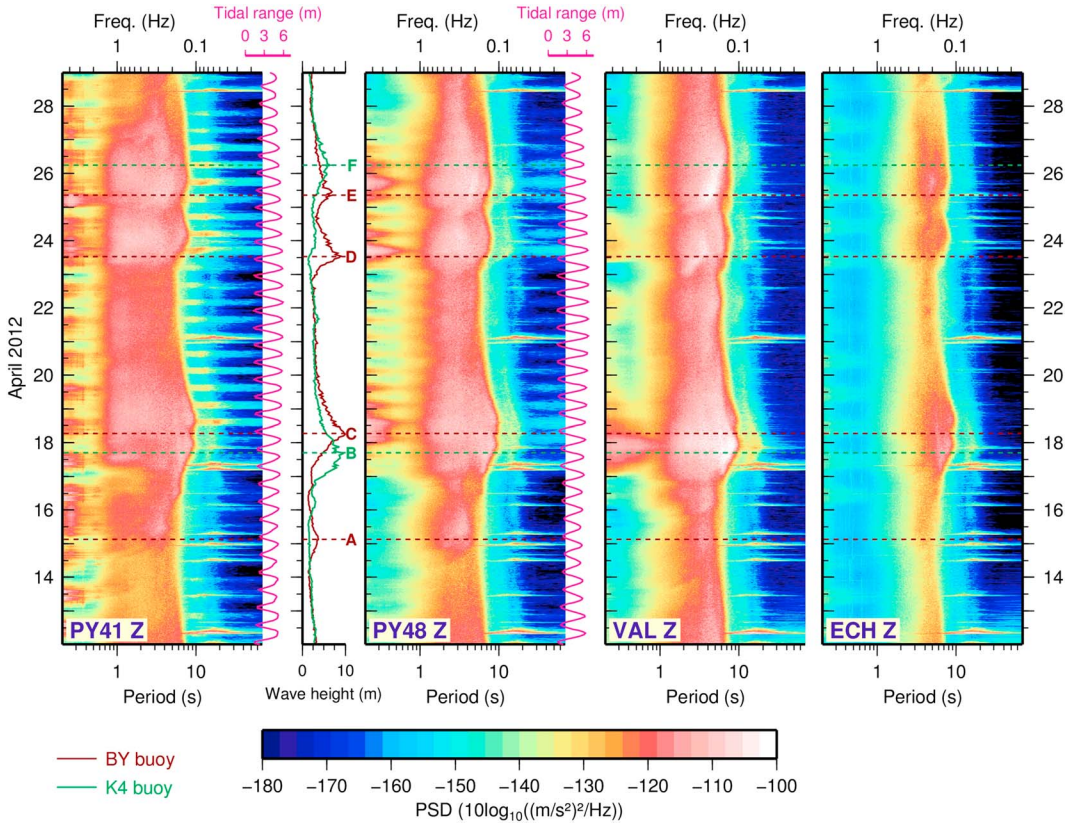

Figure 2. Vertical short-duration power spectrograms during 17 days in April 2012. Periods and frequencies are plotted on the horizontal axes (bottom and top, respectively). PSD are computed between 0.2 and 70 s period. No data selection has been performed to remove earthquakes. The local tidal ranges at PY41 and PY48 are represented by magenta curves on the right. The wave heights at Brittany (BY) and K4 buoys (Figure 1) are plotted in brown and green, respectively. The dashed lines highlight some noticeable wave events discussed in the text.

information. For the sake of clarity, we denote hereafter the 2.5–5 s and 5–10 s period bands as SPSM and LPSM (for short- and long-period secondary microseisms, respectively).

The three coastal stations exhibit a larger noise level than the inland station (ECH), especially in the SPSM band, which is significantly wider. For instance, the PSD differences between PY48 and ECH, averaged over the month of April 2012, amount to 13.2 dB at 3 s period, whereas they do not exceed 4 dB at 7.5 s period. We notice a strong correlation between wave height peaks (dashed lines, Figure 2) and the shape of the SM peak with a broadening toward long periods during storm episodes (time labels B to E). The few hour delays between the wave height maxima and the increases of both period and energy correspond to the time taken by swells to travel the distance from the buoys to the nearest shores. The energy in the 12–18 s period band (PM peak) increases in concert with ocean swell arrivals on coasts and so with the same delay times. The very short period energy variations (0.2–2 s), observed also with the same delay times, are consistent with breaking waves at local shorelines. The broadenings of SM energy toward long periods can thus be explained by "wave-wave" interactions in shallow waters, which is consistent with near-shore swell spectra as shown in Figure S3a. The identification of LPSM microseisms on Irish coasts near VAL (time label B, Figure 2) and 12 h later on Brittany shorelines near PY48 (time label C) is representative of the storm migration. At the onset of time label B, the seismometers are observing the formation of the swell in the fetch, in which short wind generated waves become progressively longer. Few hours later, the swell propagation toward the coasts induces the typical linear dispersion from long to short waves, as previously shown by *Chevrot et al.* [2007] and *Kedar* [2011]. This behavior is supported by the numerical wave models provided by Previmer project (see the Acknowledgments section). On the other hand, moderate wave height peaks (such as time label A) do not necessarily reach the shores and consequently do not produce noticeable LPSM patterns while they are visible in the SPSM window nevertheless. Viewed from ECH, wave-wave interactions at distant coasts (1300 km and 900 km for VAL and PY48, respectively) produce two

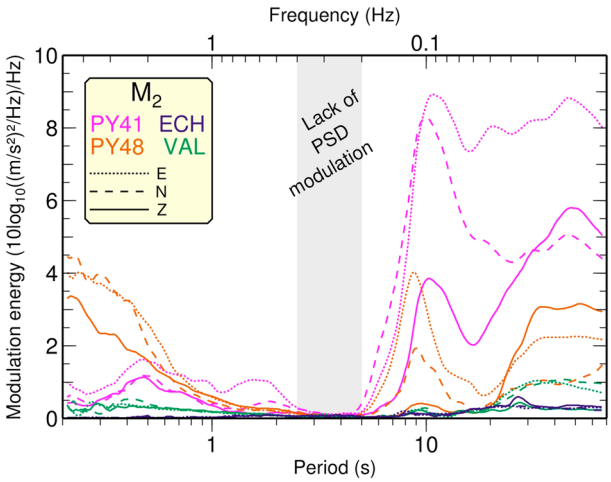

Figure 3. Energy of power spectral density modulations by the principal semidiurnal tidal component M_2. PSD time series of 225 days (10 April to 23 November 2012) are used in this computation. No normalization is applied.

very similar LPSM broadenings, the short-period energy is largely attenuated. The previous interpretations might be questioned, since SM frequencies depend on swell spectra, bathymetry, and existence of opposing waves, which is not easy to be proved when using isolated buoy data sets. We thus look for additional evidences using the strong cyclic pattern that is visible twice a day, and perfectly synchronized with local tidal range oscillations at both PY41 and PY48. High tides coincide with an increase of microseismic energy over a large spectral bandwidth and conversely, at low tides, the noise reaches minimum amplitude. At PY41 for instance, PSD values increase up to 20 dB at a 14 s period (green curve in Figure S4a). The microseismic noise at this station strongly depends on various tidal components, including shallow water harmonics. The same semidiurnal stripes are visible on the PY48 spectrogram with smaller and larger modulations at long and short periods, respectively. The horizontal spectrograms (Figures S1 and S2) show that tides (especially M_2 component) modulate the three-component microseismic energy between 0.2 s and 70 s period. While tidal modulations of the seismic signal have been previously studied mostly for IG energy [e.g., *Dolenc et al.*, 2005; *Young et al.*, 2013], we report here observations of such modulations in the microseismic 2–20 s period band. A striking feature of all spectrograms is the lack of semidiurnal stripes in the SPSM band, indicating that the high-and-low tidal cyclic modulations are extremely weak. So, since coastal microseismic sources are expected to be influenced by the tides, a distant and larger energy eclipses local tidal imprints in this spectral band.

3. M_2 Tidal Peak Modulations

The well-known 24 h modulation of the cultural noise can be superimposed on the tidal modulation, which contributes to the S_1 and S_2 peaks, as observed in Figure S4 for PY41. For this reason and because the semidiurnal M_2 tide is known to be the most energetic tidal component, we focus our tidal analysis on the seismic energy modulation at the M_2 frequency (~1.9323 cpd). For each station, M_2 modulation curves, shown in Figure 3, are computed for each component between 10 April and 23 November 2012 (225 days of continuous signal). For each period of the spectrograms shown in Figures 2, S1, and S2, the corresponding PSD values are extracted as a function of time, with a sampling rate of 0.8333 mHz (1 point every 20 min). Four PSD time series, extracted at four periods, are shown as example in Figure S4a for the vertical component at PY41. The corresponding spectral amplitudes (Figure S4b) then quantify the modulation energies of each PSD time series. In this example, it is clear that the PSD time series at 3 s (magenta curve) is not affected by the M_2 frequency, while the three other time series (extracted at 0.43, 14, and 50 s) are strongly modulated by at least two tidal peaks (M_2, S_2, and/or N_2 and other shallow water components). The M_2 modulation curves displayed in Figure 3 are constructed by computing the modulation energy at the nearest frequency from M_2 for each PSD time series defined between 0.2 and 70 s. No normalization of the modulation amplitude is applied in Figure 3. For the sake of comparison, normalized curves are displayed in Figure S5 and show the same behavior at coastal stations.

PSD time series at both VAL and ECH are weakly modulated by the M_2 frequency, with respect to PY41 and PY48 (Figure 3), although a similar V shape (with a minimum between 2 and 7 s period) can be noticed for VAL in Figure S5. Conversely, the PSD modulation curves at PY41 and PY48, both very close to the shore, confirm a large M_2 modulation of the seismic energy. At PY41, the spectrum enhances that energy depends not only on M_2 but also on various shallow water tidal components (such as M4, see Figure S4b). At PY48, the short-period modulations (lower than 1 s) can be explained by the energy of ocean waves hitting the cliff at high tides. This modulation of the short-period seismic energy is larger than the effect of the swash at

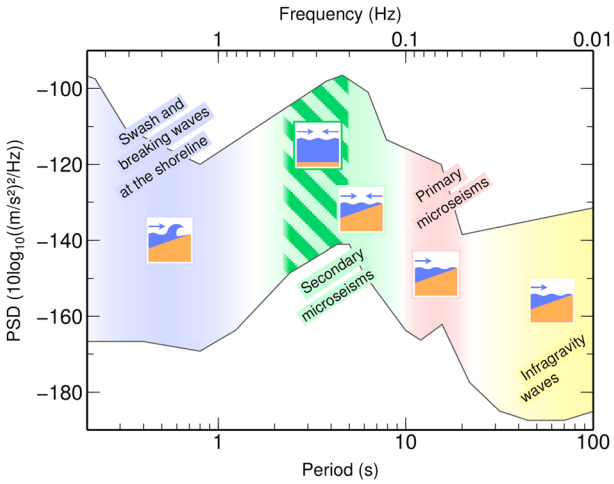

Figure 4. Summary of the ocean signature on seismic energy recorded at Atlantic shoreline stations. The open ocean-generated microseisms outshine all other energies in the period band of 2.5–5 s (SPSM, hatched green domain). Both shallow water and open ocean microseisms are due to wave-wave interactions and contribute to the secondary microseisms in their respective spectral band. The seismic energy for periods lower than 2 s (noticeable at PY48 and VAL, Figure 2) is due to the wave breaking on cliffs but also exists in swash areas, such as PY41. Black curves are the New High Noise Model and New Low Noise Model [*Peterson*, 1993].

PY41. We propose to use the strength of M_2 modulation as a proxy for in situ effects. Thus, the lack of modulation between 2.5 and 5 s at all stations and for all components (Figure 3) demonstrates that the large extra energy that is observed in this period band in Figure 2 is not M_2 frequency dependent and overprints the local microseismic energy which oscillates back and forth with the semidiurnal tides. This spectral window exactly matches half of the swell period band values recorded at BY during 2012. This observation holds at another buoy located in the Bay of Biscay, above approximately 4560 m of water height, as shown in Figure S3. This strengthens that the extra energy is due to deep ocean-generated microseisms which overcome the tidally modulated coastal microseism energy in the 2.5–5 s period band.

4. Discussion and Conclusion

We observe that continuous microseismic energy recorded at stations located on the western Europe shorelines is strongly influenced by ocean tides. This effect has been reported at other places worldwide [*Young et al.*, 2013], mostly for IG waves. It is not clear, at this stage, what is the cause of the tidal modulation of microseismic noise and the frequency range where this coupling occurs since this study is only focused on the 0.2–20 s period band. So far, we believe that the most likely explanations are tidal loading and/or tidal currents, since energy amplification cannot be explained by tilt effects only. It has been observed that IG energy (20–200 s period) is tidally modulated near the shorelines, where tidal variations of the surf zone affect the generation, the dissipation, and the reflection of IG waves [*Okihiro and Guza*, 1995]. *Thomson et al.* [2006] showed that IG energy can be transferred back to higher-frequency motions, and these nonlinear interactions depend on the bathymetric profile of the surf zone, perpetually modified by high-and-low tide cycles. It has not been shown whether this nonlinear transfers of energy can occur as well in the 2–20 s period band. In any case, tidal modulations can be used as proxy for near-shore microseism generation and hence can be used to quantify coastal reflection coefficients, as a function of frequency (Figure S6), in numerical models [e.g., *Ardhuin et al.*, 2011].

The mechanisms for SM generation are complex and may vary from one ocean to another. There is a broad and continuous spectrum of ocean waves that generates a corresponding spectrum of seismic energy depending on seasons, ocean conditions and bathymetry [*Kedar et al.*, 2008], and attenuation between SM source location and seismometers. We have demonstrated that tide also have a strong influence on microseisms generated in shallow waters. Microseisms coming from the North Atlantic ocean and recorded in the western Europe are of two types: SPSM (2.5–5 s) generated in open sea and SM (2.5–10 s) produced in the coastal regions, although each period domain can obviously vary according to the swell spectra. We do not argue that coastal SM has no energy in the 2.5–5 s period band, we simply observe that it is eclipsed by deep-ocean SPSM energy, as sketched in Figure 4. When considering swell spectra near the coastline (Figure S3) SM should occur in the well-known 2–10 s period band, but, due to the locations of seismic stations, the remote SPSM energy is less attenuated, as classically observed. The existence of deep water-generated microseisms is now established [*Bromirski et al.*, 2005], although they are not easily highlighted in the inland background seismic noise [*Bromirski et al.*, 2013; *Ying et al.*, 2014]. We compare the swell height variations at BY during 115 days in 2012 and two PSD time series, extracted at 3.33 s (central value for SPSM window) at PY41 and ECH (Figure S7). The strong correlation between PY41 and ECH curves (normalized correlation coefficient of 0.92) tends to indicate that SPSM open sea-generated

microseisms are detectable 700 km away from the coast, but with a larger attenuation of the energy during propagation in the continental crust. At places where such SPSM exist, both coastal and inland seismometers can find usefulness for presatellite ocean activity reconstruction. Ambient noise seismology can also benefit from this result for both tomography and monitoring purposes [*Shapiro et al.*, 2005; *Brenguier et al.*, 2008], since the origin of noise sources can influence the cross-correlation reconstruction. Finally, this observation may also contribute to map the opposing wave locations in the case of storms migrating toward shorelines, using coastal seismometers, in addition to buoy and satellite data and so to estimate the storm power. For instance, observations of microseismic signals in Florida (station O62Z, see Figure 3 in *Sufri et al.* [2014]), clearly display short-period microseisms generated by superstorm Sandy at late 21 October 2012. If SPSM overprint also exists in the central western Atlantic Ocean, the noticeable energy in the 2.5–5 s can be linked to deep-ocean activity which occurred a few hours before the National Hurricane Center upgraded Sandy as a tropical storm.

Acknowledgments

The Atlantic station deployment would not have been possible without the help of the municipalities of Camaret-sur-mer (PY48) and Le-Château-d'Oléron (PY41). The PYROPE data set is archived by Geodata team of ISTerre (Grenoble). PY41 and PY48 are now RESIF permanent stations (UNCO and CAMF, respectively), and data are freely available (http://www.resif.fr). ECH is a Geoscope station, and authors would like to thank Sergei Lebedev for providing VAL continuous data. Figures are produced using GMT [*Wessel et al.*, 2013], and our data processing codes use "The Fastest Fourier Transform of the West" [*Frigo and Johnson*, 2005] libraries. The buoy data were collected and made freely available by the CDOCO in the framework of Previmer project and programs that contribute to it (http://www.previmer.org). This work is supported by the ANR-09-0229-000 (PYROPE project), VIBRIS project (Council of Pays de la Loire), and by the Nantes-Atlantique Observatory (OSUNA). M. Schimmel acknowledges support by Topolberia (CSD2006-00041) and CGL2013-48601-C2-1-R. We would like to thank the Editor, an anonymous reviewer, and Sharon Kedar for very constructive comments. In memory of Olivier Quillard who installed and maintained PYROPE stations.

The Editor thanks two anonymous reviewers for their assistance in evaluating this paper.

References

Ardhuin, F., and H. C. Herbers (2013), Noise generation in the solid earth, oceans and atmosphere, from nonlinear interacting surface gravity waves in finite depth, *J. Fluid Mech.*, *716*, 316–348.

Ardhuin, F., E. Stutzmann, M. Schimmel, and A. Mangeney (2011), Ocean wave sources of seismic noise, *J. Geophys. Res.*, *116*, C09004, doi:10.1029/2011JC006952.

Aster, R. C., D. E. McNamara, and P. D. Bromirski (2008), Multidecadal climate-induced variability in microseisms, *Seismol. Res. Lett.*, *79*(2), 194–202, doi:10.1785/gssrl.79.2.194.

Bernard, P. (1990), Historical sketch of microseisms from past to future, *Phys. Earth Planet. Inter.*, *63*(3–4), 145–150.

Bertelli, T. (1872), Osservazioni sui piccoli movimenti dei pendoli in relazione ad alcuni fenomeni meteorologiche, *Boll. Meteorol. Osserv. Coll. Roma*, *9*, 19.

Brenguier, F., N. Shapiro, M. Campillo, V. Ferrazzini, Z. Duputel, O. Coutant, and A. Nercessian (2008), Towards forecasting volcanic eruptions using seismic noise, *Nat. Geosci.*, *1*(2), 126–130.

Bromirski, P. D., and F. K. Duennebier (2002), The near-coastal microseism spectrum: Spatial and temporal wave climate relationships, *J. Geophys. Res.*, *107*(B8), 2166, doi:10.1029/2001JB000265.

Bromirski, P. D., F. K. Duennebier, and R. A. Stephen (2005), Mid-ocean microseisms, *Geochem. Geophys. Geosyst.*, *6*, Q04009, doi:10.1029/2004GC000768.

Bromirski, P. D., R. A. Stephen, and P. Gerstoft (2013), Are deep-ocean-generated surface-wave microseisms observed on land?, *J. Geophys. Res. Solid Earth*, *118*, 3610–3629, doi:10.1002/jgrb.50268.

Cessaro, R. K. (1994), Sources of primary and secondary microseisms, *Bull. Seismol. Soc. Am.*, *84*(1), 142–148.

Chevrot, S., M. Sylvander, S. Benahmed, C. Ponsolles, J. M. Lefèvre, and D. Paradis (2007), Source locations of secondary microseisms in western Europe: Evidence for both coastal and pelagic sources, *J. Geophys. Res.*, *112*, B11301, doi:10.1029/2007JB005059.

Chevrot, S., et al. (2014), High-resolution imaging of the Pyrenees and Massif Central from the data of the PYROPE and IBERARRAY portable array deployments, *J. Geophys. Res. Solid Earth*, *119*, 6399–6420, doi:10.1002/2014JB010953.

Dolenc, D., B. Romanowicz, D. Stakes, P. McGill, and D. Neuhauser (2005), Observations of infragravity waves at the Monterey ocean bottom broadband station (MOBB), *Geochem. Geophys. Geosyst.*, *6*, Q09002, doi:10.1029/2005GC000988.

Ebeling, C. W. (2012), Chapter one—Inferring ocean storm characteristics from ambient seismic noise: A historical perspective, in *Advances in Geophysics*, vol. 53, edited by R. Dmowska, pp. 1–33, Elsevier.

Frigo, M., and S. G. Johnson (2005), The design and implementation of FFTW3, *Proc. IEEE*, *93*(2), 216–231, special issue on "Program Generation, Optimization, and Platform Adaptation".

Fund, F., L. Morel, and A. Mocquet (2012), Assessment of the FES2004 derived OTL model in the west of France and preliminary results about impacts of tropospheric models, in *Geodesy for Planet Earth, International Association of Geodesy Symposia*, vol. 136, edited by S. Kenyon, M. C. Pacino, and U. Marti, pp. 573–579, Springer, Berlin, doi:10.1007/978-3-642-20338-1_70.

Gerstoft, P., and T. Tanimoto (2007), A year of microseisms in southern California, *Geophys. Res. Lett.*, *34*, L20304, doi:10.1029/2007GL031091.

Hasselmann, K. (1963), A statistical analysis of the generation of microseisms, *Rev. Geophys.*, *1*(2), 177–210.

Haubrich, R., and K. McCamy (1969), Microseisms: Coastal and pelagic sources, *Rev. Geophys.*, *7*, 539–571.

Kedar, S. (2011), Source distribution of ocean microseisms and implications for time-dependent noise tomography, *C. R. Geosci.*, *343*(8–9), 548–557.

Kedar, S., M. Longuet-Higgins, F. Webb, N. Graham, R. Clayton, and C. Jones (2008), The origin of deep ocean microseisms in the north Atlantic ocean, *Proc. R. Soc. A*, *464*(2091), 777–793, doi:10.1098/rspa.2007.0277.

Kobayashi, N., and K. Nishida (1998), Continuous excitation of planetary free oscillations by atmospheric disturbances, *Nature*, *395*, 357–360, doi:10.1038/2642.

Llubes, M., et al. (2008), Multi-technique monitoring of ocean tide loading in northern France, *C. R. Geosci.*, *340*(6), 379–389.

Longuet-Higgins, M. S. (1950), A theory of the origin of microseisms, *Philos. Trans. R. Soc. London*, *243*(857), 1–35.

McNamara, D. E., and R. Boaz (2006), Seismic noise analysis system using power spectral density probability density functions: A stand-alone software package, *U.S. Geol. Surv. Open File Rep., 2005–1438*.

Obrebski, M. J., F. Ardhuin, E. Stutzmann, and M. Schimmel (2012), How moderate sea states can generate loud seismic noise in the deep ocean, *Geophys. Res. Lett.*, *39*, L11601, doi:10.1029/2012GL051896.

Okihiro, M., and R. T. Guza (1995), Infragravity energy modulation by tides, *J. Geophys. Res.*, *100*(C8), 16,143–16,148.

Oliver, J., and R. Page (1963), Concurrent storms of long and ultralong period microseisms, *Bull. Seismol. Soc. Am.*, *53*(1), 15–26.

Peterson, J. (1993), Observations and modelling of seismic background noise, *U.S. Geol. Surv. Open File Rep., 93 –322*.

Rhie, J., and B. Romanowicz (2004), Excitation of Earth's continuous free oscillations by atmosphere ocean seafloor coupling, *Nature*, *431*, 552–556.

Romanowicz, B., M. Cara, J.-F. Fels, and D. Rouland (1984), Geoscope: A French initiative in long period three component seismic networks, *Eos Trans. AGU*, *65*, 753–754.
Schimmel, M., E. Stutzmann, F. Ardhuin, and J. Gallart (2011), Polarized Earth's ambient microseismic noise, *Geochem. Geophys. Geosyst.*, *12*, Q07014, doi:10.1029/2011GC003661.
Sergeant, A., E. Stutzmann, A. Maggi, M. Schimmel, F. Ardhuin, and M. Obrebski (2013), Frequency-dependent noise sources in the north Atlantic Ocean, *Geochem. Geophys. Geosyst.*, *14*, 5341–5353, doi:10.1002/2013GC004905.
Shapiro, N. M., M. Campillo, L. Stehly, and M. H. Ritzwoller (2005), High-resolution surface-wave tomography from ambient seismic noise, *Science*, *307*(5715), 1615–1618, doi:10.1126/science.1108339.
Stephen, R. A., F. N. Spiess, J. A. Collins, J. A. Hildebrand, J. A. Orcutt, K. R. Peal, F. L. Vernon, and F. B. Wooding (2003), Ocean seismic network pilot experiment, *Geochem. Geophys. Geosyst.*, *4*(10), 1092, doi:10.1029/2002GC000485.
Stutzmann, E., M. Schimmel, G. Patau, and A. Maggi (2009), Global climate imprint on seismic noise, *Geochem. Geophys. Geosyst.*, *10*, Q11004, doi:10.1029/2009GC002619.
Stutzmann, E., F. Ardhuin, M. Schimmel, A. Mangeney, and G. Patau (2012), Modelling long-term seismic noise in various environments, *Geophys. J. Int.*, *191*(2), 707–722, doi:10.1111/j.1365-246X.2012.05638.x.
Sufri, O., K. D. Koper, R. Burlacu, and B. de Foy (2014), Microseisms from superstorm Sandy, *Earth Planet. Sci. Lett.*, *402*, 324–336, special issue on {USArray} science.
Tanimoto, T. (2007), Excitation of microseisms, *Geophys. Res. Lett.*, *34*, L05308, doi:10.1029/2006GL029046.
Thomson, J., S. Elgar, B. Raubenheimer, T. H. C. Herbers, and R. T. Guza (2006), Tidal modulation of infragravity waves via nonlinear energy losses in the surfzone, *Geophys. Res. Lett.*, *33*, L05601, doi:10.1029/2005GL025514.
Webb, S. C. (1998), Broadband seismology and noise under the ocean, *Rev. Geophys.*, *36*(1), 105–142, doi:10.1029/97RG02287.
Webb, S. C. (2007), The Earth's "hum" is driven by ocean waves over the continental shelves, *Nature*, *445*, 754–756, doi:10.1038/nature05536.
Wessel, P., W. H. F. Smith, R. Scharroo, J. Luis, and F. Wobbe (2013), Generic Mapping Tools: Improved version released, *Eos Trans. AGU*, *94*(45), 409–410, doi:10.1002/2013EO450001.
Wiechert, E. (1904), Verhandlugen der zweiten internationalen seismologischen konferenz, *Gerlands Beitr. Geophys.*, *2*, 41–43.
Ying, Y., C. J. Bean, and P. D. Bromirski (2014), Propagation of microseisms from the deep ocean to land, *Geophys. Res. Lett.*, *41*, 6374–6379, doi:10.1002/2014GL060979.
Young, A. P., R. T. Guza, M. E. Dickson, W. C. O'Reilly, and R. E. Flick (2013), Ground motions on rocky, cliffed, and sandy shorelines generated by ocean waves, *J. Geophys. Res. Oceans*, *118*, 6590–6602, doi:10.1002/2013JC008883.